Journal of The Electrochemical Society

The Electrochemical Society
Advancing solid state & electrochemical science & technology

OPEN ACCESS

High Power and High Capacity 3D-Structured TiO_2 Electrodes for Lithium-Ion Microbatteries

To cite this article: Jie Xie *et al* 2016 *J. Electrochem. Soc.* **163** A2385

View the article online for updates and enhancements.

ECS Membership = Connection

ECS membership connects you to the electrochemical community:

- Facilitate your research and discovery through ECS meetings which convene scientists from around the world;
- Access professional support through your lifetime career:
- Open up mentorship opportunities across the stages of your career;
- Build relationships that nurture partnership, teamwork—and success!

Join ECS! Visit electrochem.org/join

This content was downloaded from IP address 122.107.103.56 on 21/08/2022 at 21:27

Journal of The Electrochemical Society, **163** (10) A2385-A2389 (2016)

High Power and High Capacity 3D-Structured TiO_2 Electrodes for Lithium-Ion Microbatteries

Jie Xie,[a] Jos F. M. Oudenhoven,[b] Dongjiang Li,[a,*] Chunguang Chen,[a,c] Rüdiger-A. Eichel,[c,d] and Peter H. L. Notten[a,c,,z]**

[a]*Eindhoven University of Technology, 5600 MB Eindhoven, The Netherlands*
[b]*Holst Centre - imec, 5656 AE Eindhoven, The Netherlands*
[c]*Forschungszentrum Jülich (IEK-9), D-52425 Jülich, Germany*
[d]*RWTH Aachen University, D-52074 Aachen, Germany*

An on-chip compatible method to fabricate high energy density TiO_2 thin film electrodes on 3D-structured silicon substrates was demonstrated. 3D-structured electrodes are fabricated by combining reactive ion etching (RIE) with low pressure chemical vapor deposition (LPCVD), enabling accurate control of the aspect ratio of substrates and the subsequent deposition of TiO_2 thin film electrodes onto these structured substrates. The prepared 3D-TiO_2 electrodes exhibit a current-dependent increase in storage capacity of a factor up to 16 as compared to conventional planar electrodes. In addition, these 3D electrodes also reveal excellent power and cycling performance. This work demonstrates that LPCVD is capable of depositing homogeneous film electrodes on highly structured substrates and the prepared 3D-electrodes also shows significant improve in storage capacity and power density.
© The Author(s) 2016. Published by ECS. This is an open access article distributed under the terms of the Creative Commons Attribution Non-Commercial No Derivatives 4.0 License (CC BY-NC-ND, http://creativecommons.org/licenses/by-nc-nd/4.0/), which permits non-commercial reuse, distribution, and reproduction in any medium, provided the original work is not changed in any way and is properly cited. For permission for commercial reuse, please email: oa@electrochem.org. [DOI: 10.1149/2.1141610jes]
All rights reserved.

Manuscript submitted June 24, 2016; revised manuscript received August 8, 2016. Published September 1, 2016.

Nowadays, many electronic products are becoming smart and connected. Thousands of wireless sensors united in networks collect useful data that make our lives safer and more convenient. As sensors, wireless communication devices, personal health monitoring systems and autonomous microelectromechanical systems (MEMS) become more widespread and individual sensor nodes become more compact,[1–5] there is an increasing demand for integrated power sources. Typically, there is a demand for batteries in the $1 \sim 10$ mm^3 volume range, including all components and associated packaging.[6] Moreover, for use in miniaturized devices, it is usually required that the energy storage functions are physically located on a small chip area. A miniaturized on-chip battery would be highly desirable for these applications, making the energy and power density per footprint area a key attribute of these batteries.

Conventional 2D thin film microbatteries can deliver high power, but require large footprint areas to store reasonable energies. On the other hand, making the electrodes thicker boosts the theoretical areal energy density but the resultant increase in electronic and ionic diffusion lengths reduces the effective power. This energy and power dilemma is schematically shown in Fig. 1. The most promising way to combine a high storage capacity and high power capability on a limited area is to integrate all battery components, i.e. current collectors, electrodes and electrolyte, in a 3-dimensional (3D) arrangement, thus generating a 3D microbattery (Fig. 1).[7–11] Due to the large surface area of these electrodes, high capacities per footprint area can be obtained. High power capabilities can also be realized by carefully designing the battery to obtain short transport distances between the electrodes.[12,13] It is important to recognize that for small electronic- and MEMS-type devices, the available area is limited. Traditional performance indicators of batteries, namely gravimetric, volumetric energy and power densities are therefore less relevant. Instead, the real issue is how much energy and power a device can deliver per footprint area, measured in terms of $mAh \cdot cm^{-2}$, $J \cdot cm^{-2}$ or $\mu W \cdot mm^{-2}$, etc.[14]

TiO_2 has been considered as a promising electrode for Li-ion batteries as it is safe, non-toxic, readily available and long cycle stability. However, the poor conductivity and slow diffusion rate of Li^+ in TiO_2 has restricted the rate capability and storage capacity of TiO_2.[15,16] A potential solution to overcome this limitation is simply by decreasing the thin film thickness. However, nano-sizing the film thickness typically leads to severe capacity reduction. Employing 3D-TiO_2 thin film electrodes is, however, a promising method to solve this dilemma.[17–19]

Several reports have demonstrated that 3D-TiO_2 electrodes reveal a higher footprint areal storage capacity and power performance.[17,18,20–22] However, since these methods are not directly based on Si substrate technology, integrating these 3D batteries onto chips or micro-sensors would be very challenging. Besides, in some work, the applied deposition method is atomic layer deposition (ALD).[17,18,20] The ALD processes are complicated and the growth rate is slow, limiting large scale production. Reactive ion etching (RIE) and low pressure chemical vapor deposition (LPCVD) are two commonly used techniques in the semiconductor industry. The RIE method is very convenient in creating periodically micro-structured 3D substrates with high aspect ratios and LPCVD is capable of producing high quality, high-performance thin films.[23–25] Here, we report a flexible and on-chip 3D microbatteries by combining the techniques of RIE with LPCVD. Two kinds of 3D-structured substrates with varying

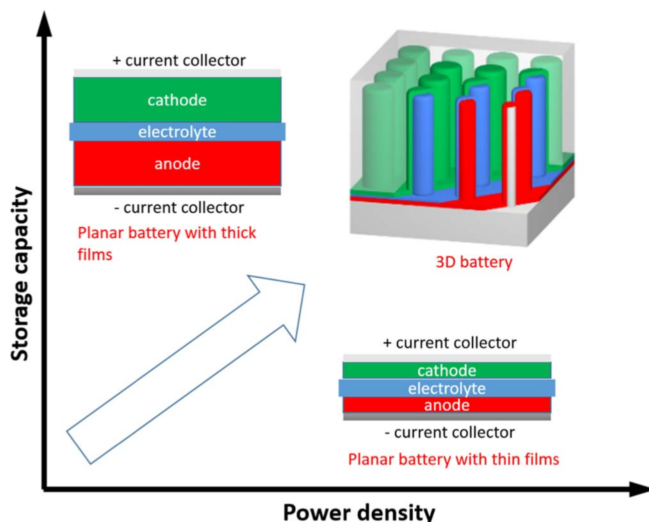

Figure 1. Design of a 3D microbattery and its advantages compared with planar microbatteries.

*Electrochemical Society Student Member.
**Electrochemical Society Member.
[z]E-Mail: p.h.l.notten@tue.nl

aspect ratios have been investigated. One kind of 3D substrate is Si trenches; the other is Si pillars. Trench substrates are convenient to prepare samples for cross-section view to check the uniformity of deposited films. Due to more open space, Si pillar substrates are more convenient for mass production and easy to be coated with other films. In this study, for the first time, homogeneous 3D-TiO_2 thin film electrodes are deposited by LPCVD in 3D Si trenches and on Si pillar substrates. The energy and power densities and cycle life of these 3D-structured TiO_2 electrodes are investigated.

Experimental

Thin film deposition.—(100) oriented silicon wafers were used as starting material. In order to increase the effective surface area of the Si substrates, etching of trenches with aspect ratios of 1 and 3 and Si pillars with length of 50 μm was conducted using photolithography and RIE, of which the parameters were published before.[26] The MOCVD setup used for TiO_2 deposition has been described in detail in a previous publication.[23] In short, a cold wall MOCVD reactor (Aixtron 200 RF) was used, in which the substrate was positioned on a radio frequency heated susceptor. The precursor was titanium(IV) isoproxide (TTIP), acquired from SAFC-Hitech (United Kingdom). TTIP was delivered in a stainless steel bubbler. This bubbler was thermostated at 25°C, and the pressure was controlled at 300 mbar. The flow rate of argon through the bubbler to evaporate TTIP was fixed at 100 sccm, while the total flow through the reactor was 1550 sccm. The deposition temperature was varied from 350 to 550°C. Argon was used as carrier gas. The pressure of the reactor was 5 mbar during the deposition processes.

TiO_2 films for thickness and surface morphology analyses were deposited onto square silicon substrates with a width of 3 cm. The planar TiO_2 electrodes prepared for electrochemical measurements were deposited on similar substrates covered with an adhesive barrier layer of TiN (30 nm) and a layer of platinum (70 nm) as current collector. To investigate the uniformity of the 3D deposition, TiO_2 films were deposited onto structured silicon substrates, in which trenches with a depth of 30 μm and width of 30 and 10 μm were etched with RIE, as shown in Figs. 2a and 2b, respectively. To investigate the electrochemical performance of 3D-TiO_2 electrodes, the films were deposited on silicon into which a pillar structure was etched.

The pillars were coated with 30 nm TiN by ALD, which was used as current collector. The diameter and height of the Si pillars are 2 μm and 50 μm, respectively, and the distance between pillars is 5 μm. SEM images of these pillar substrates are shown in Figs. 2c and 2d. The surface enlarging factor (A) of the pillar substrate used for the electrochemical investigations is calculated, according to

$$A = 1 + \pi dh/(d + l)^2 \quad [1]$$

where d and h represent the diameter and length of pillars, respectively. l is the distance between Si pillars.

Sample characterization.—The thickness and morphology of the TiO_2 thin films were analyzed, using a scanning electron microscope (SEM, Philips/FEI XL 40 FEG). Measurements of Raman spectra were performed on an Olympus BX40 Raman Spectrometer under a backscattering geometry. A 633 nm line of a Helium-Neon laser was taken as the excitation source. The electrochemical measurements were performed in an argon-filled glove box (O_2 and H_2O < 1 ppm). The samples were positioned in Teflon cells and used as working electrodes. Lithium metal foils were utilized as reference and counter electrodes. The cell was filled with 1 M $LiClO_4$ in propylene carbonate (Soulbrain MI, United States) as electrolyte. This three-electrode setup was connected to a M2300 galvanostat (Maccor, Tulsa, USA) to perform galvanostatic (dis)charging from 0 to 3 V vs. Li/Li^+ at different current densities: 4, 8, 20, 40 and 80 μA per cm^2 footprint area. All electrochemical tests were carried out at room temperature (∼22°C).

Results and Discussion

The SEM images of TiO_2 films deposited at different temperatures are shown in Figs. 3a–3d. It is clear that all films are homogeneous without revealing any cracks or pinholes, which is an apparent advantage of LPCVD to deposit high quality thin films. The simplicity of the deposition process also permits the processing of large wafer batch sizes. It is interesting to note that the thicknesses of films deposited at higher temperatures, 400, 450 and 550°C, are close to each other, but much thicker than the films deposited at 350°C, which indicates a significant increase of growth rate from 350 to 400°C.

The Raman spectra of the deposited films are shown in Fig. 4 as a function of deposition temperature. The Raman spectra of the four films are very similar to each other, showing small peaks at 396 and 639 cm^{-1} and very sharp and intense peak at 144 cm^{-1}, which match well with the reported Raman bands for anatase.[27] It can therefore be concluded that all deposited TiO_2 films have the anatase structure.

Fig. 5 shows the Arrhenius plot of the growth of planar TiO_2 films. It is obvious that the growth of TiO_2 films can be divided into two parts,

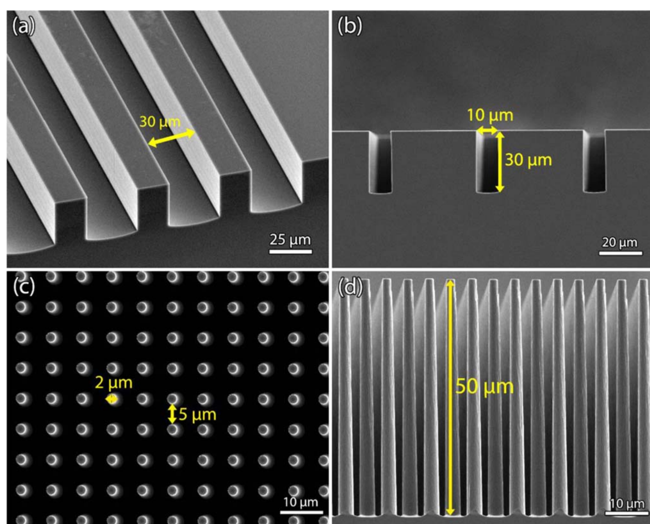

Figure 2. SEM images of tilt view of a 30 μm wide trench (a); cross-section view of a 10 μm wide trench (b); top (c) and cross-section view (d) of a 3D pillar substrate.

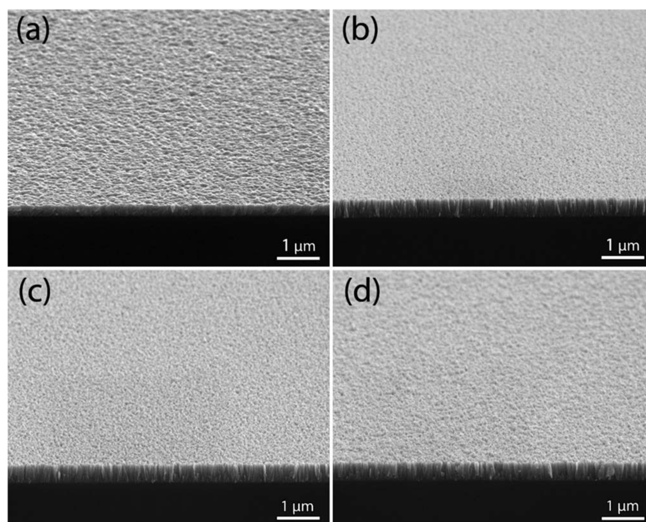

Figure 3. SEM images of TiO_2 films deposited at 350 (a), 400 (b), 450 (c) and 550 (d)°C, respectively.

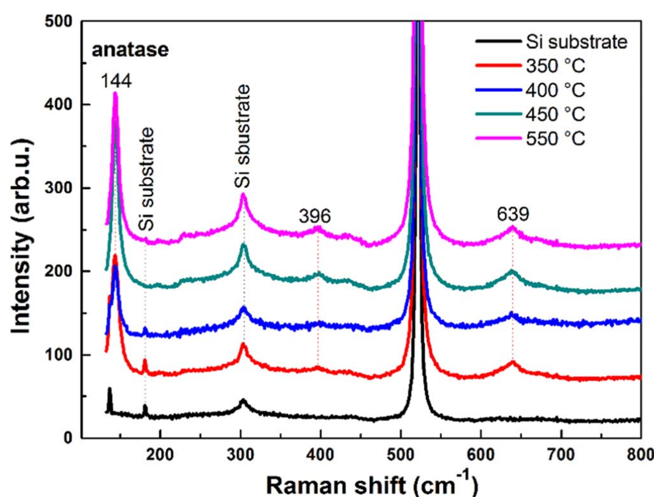

Figure 4. Raman spectroscopy of TiO_2 films deposited at various temperatures.

indicating that there are two different rate-determining processes in these temperature ranges. At high temperatures the deposition rate is only weakly dependent on the deposition temperature. Increasing the deposition temperature from 450 to 550°C only result in a small increase of growth rate, which indicates that in this temperature range the growth of TiO_2 is a diffusion controlled process.[28] In contrast, in the low-temperature region where the slope in Fig. 5 is much steeper, the deposition rate is strongly dependent on the temperature. Here, the activation energy calculated from Fig. 5 is 63.4 kJ/mole, which is relatively high, indicating the deposition of TiO_2 at 350°C is a kinetically controlled process.[28] Therefore, it was concluded that the deposition rate was limited by diffusive transport in the high-temperature range, while at lower temperatures the deposition is a kinetically controlled process. Within the kinetically controlled region, the growth rate is relatively slow, implying that the chemical conversion of Ti-precursor during the transportation of precursor gas into trenches is slow. Thus, there will still be sufficient Ti-precursor available for the growth of the TiO_2 film even toward the bottom of the trench. A uniform deposition at different parts of the 3D substrate can therefore be expected under these conditions.

Figs. 6a–6c shows a TiO_2 film deposited on different sections (I, II, III and IV) of a 10 μm wide trench. The applied deposition temperate is 350°C, clearly within the kinetically controlled temperature region. Obviously, the deposited film is very homogeneous from top to bottom. Fig. 6d shows the development of deposited film thickness as a function of distance from the top surface to the bottom on two trench substrates with different widths, 30 and 10 μm. For both trenches, the films deposited on the top part of the substrates are around 287 nm thick and slightly thinner at bottom, indicating a very high step coverage. Consistent with the prediction from the Arrhenius plot, the film deposited at 350°C is very uniform.

To show the advantages of 3D-electrodes in improving both the capacity and power performances, TiO_2 thin film electrodes have been deposited on TiN-covered 3D micro-pillar substrates to investigate the electrochemical performances. Fig. 7a shows the tilt-view of a pillar substrate. Based on geometrical calculations, the surface area enlargement factor is 7.4. Figs. 7b–7d show the film thickness distribution

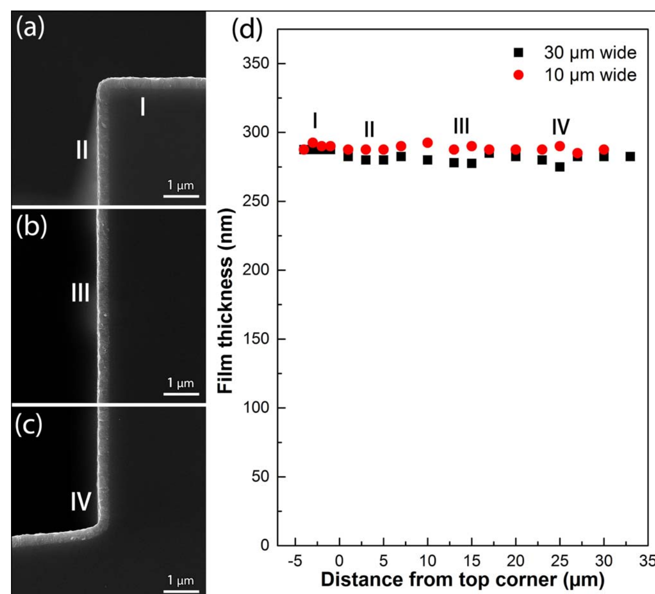

Figure 6. SEM images of deposited TiO_2 films on top (a), middle (b) and bottom (c) part of a 10 μm trench; the development of deposited TiO_2 film thickness as a function of distance from the top surface (d). The applied deposition temperature is 350°C.

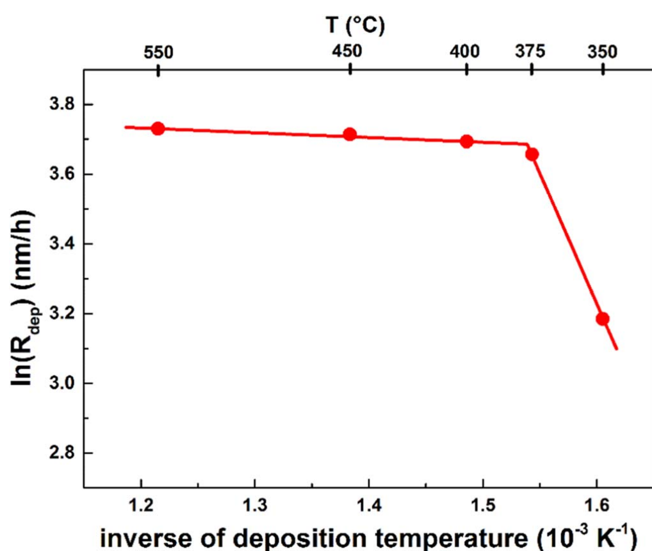

Figure 5. Arrhenius plot for the deposition of planar TiO_2 film.

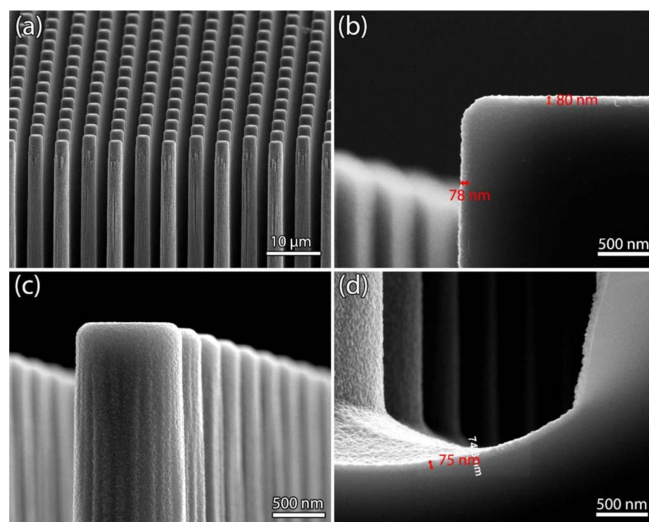

Figure 7. Tilt view of 3D pillar substrates covered by TiO_2 (a), SEM images of deposited TiO_2 film on top (b), surface (c) and bottom (d) part of a 3D pillar substrate. The applied deposition temperature is 350°C.

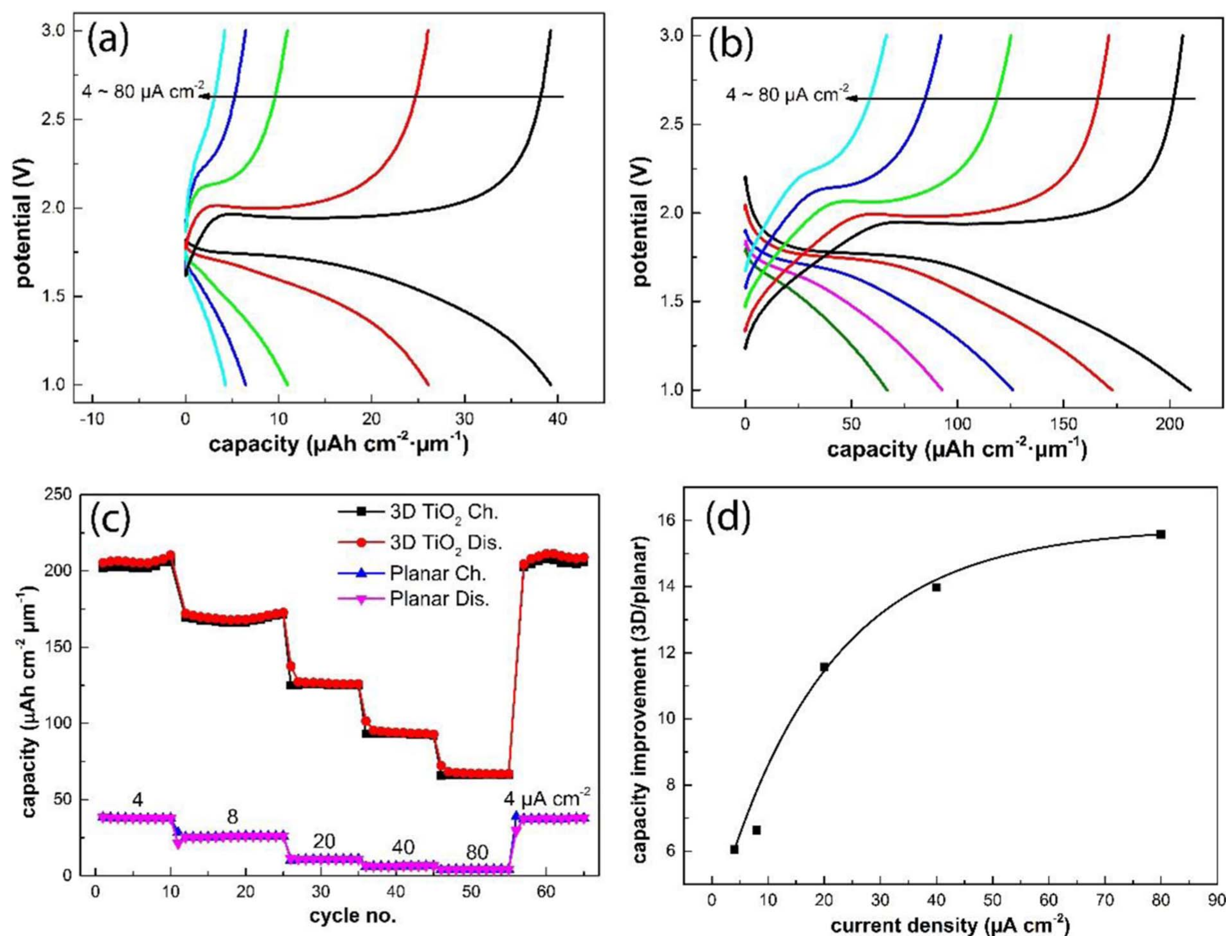

Figure 8. Voltage curves of planar TiO_2 (a) and 3D TiO_2 electrodes (b); Areal capacity of planar and 3D TiO_2 electrodes for charging (Ch.) and discharging (Dis.) at different current densities (c); areal capacity improvement as a function of current densities (d).

of a TiO_2 film deposited at 350°C on the surface of Si pillars. A film with layer thickness of 80 nm is deposited on the top surface. At the bottom of the Si pillars, the film thickness is 75 nm. A step coverage of 94% was achieved.

For LPCVD, the deposited film thickness increases linearly with deposition time.[24] The thickness of TiO_2 electrodes can be easily adjusted by changing the deposition time. In order to achieve a high power performance, thin TiO_2 films (40 nm) were choosing as demonstrator. The voltage curves of a planar and a 3D-structured TiO_2 electrode at different (dis)charging current densities are shown in Figs. 8a and 8b, respectively. For these electrodes, the typical (dis)charging behavior of anatase TiO_2 is shown. Voltage plateaus at ~1.7 and ~2.0 V were observed in the charge-discharge curves of both planar and 3D TiO_2 film anodes, which can be attributed to the insertion and extraction of Li^+ through Li-poor tetrahedral TiO_2 and the Li-rich orthorhombic $Li_{0.6}TiO_2$, respectively.[29] Although more Li can be accommodated in $Li_{0.6}TiO_2$ to form $LiTiO_2$ by further two-phase intercalation, the reaction is known to have sluggish kinetics.[16,30] For bulk TiO_2 (>40 nm), the theoretical capacity is 201 mAh/g ($Li_{0.6}TiO_2$)[16,30] or 782 $mAh \cdot cm^{-3}$, considering the density of anatase to be 3.89 $g \cdot cm^{-3}$. Therefore, the theoretical area capacity is 78.2 $\mu Ah \cdot cm^{-2} \cdot \mu m^{-1}$ for a 1 μm thick TiO_2 film electrode. For a 40 nm planar electrode, 1 C equals to $78.2 \times 0.04 = 3.1$ $\mu A\ cm^{-2}$. So, the (dis)charging current densities of 4 and 80 $\mu A \cdot cm^{-2}$ correspond to a 1.3 and 25.8 C-rate for planar electrodes, respectively. It is noticed that the overpotentials of 3D TiO_2 electrode are smaller than for planar electrodes, especially at high (dis)charging current density, which indicates that 3D TiO_2 electrode have better power performance.

As shown in Fig. 8c, at all applied current densities, the 3D electrode shows much higher storage capacities than the planar electrode. For a planar TiO_2 electrode the storage capacity quickly decreases with increasing (dis)charging current. At 80 $\mu A \cdot cm^{-2}$, the storage capacity has dropped to 4.1 $\mu Ah \cdot cm^{-2} \cdot \mu m^{-1}$, which is less than 14% of the initial capacity. Contrastingly, the storage capacity of the 3D-TiO_2 electrode measured at 80 $\mu A \cdot cm^{-2}$ is 66.2 $\mu Ah \cdot cm^{-2} \cdot \mu m^{-1}$, which is 16 times higher than that of the planar electrode at the same current density. It is also worthwhile to note that even at the highest current density applied (80 $\mu A \cdot cm^{-2}$), the capacity of the 3D electrode is still twice as high as the storage capacity of the planar electrode at low current densities, i.e. at 4 $\mu A \cdot cm^{-2}$. Obviously, the power performance per footprint area of TiO_2 is significantly improved by the 3D-structure.

For the 3D-electrodes, the surface area is enlarged by 7.4 times, which means that 7.4 times more TiO_2 has been deposited within the same footprint area compared to planar electrodes. Therefore, for 3D-electrodes, a 1 C-rate equals to $78.2 \times 0.04 \times 7.4 = 23.1$ $\mu A \cdot cm^{-2}$. For current density of 80 $\mu A \cdot cm^{-2}$, the C-rate for 3D-electrodes is $80/23.1 = 3.5$ C. Obviously, under the same output power, the actual C-rate of 3D-electrodes is much lower than for planar-electrodes, resulting in a better power performance. This improvement becomes more pronounced at high output powers. As shows in Fig. 8d, the storage capacity improvement of 3D electrodes with respect to planar electrodes is more significant as the current density increases. At 4 $\mu A \cdot cm^{-2}$, the storage capacity of the 3D electrode is 6 times higher than that of the planar electrode, which is smaller than the theoretical surface area enlargement of 7.4. As the applied (dis)charge current density increases, the capacity improvement of the 3D electrode

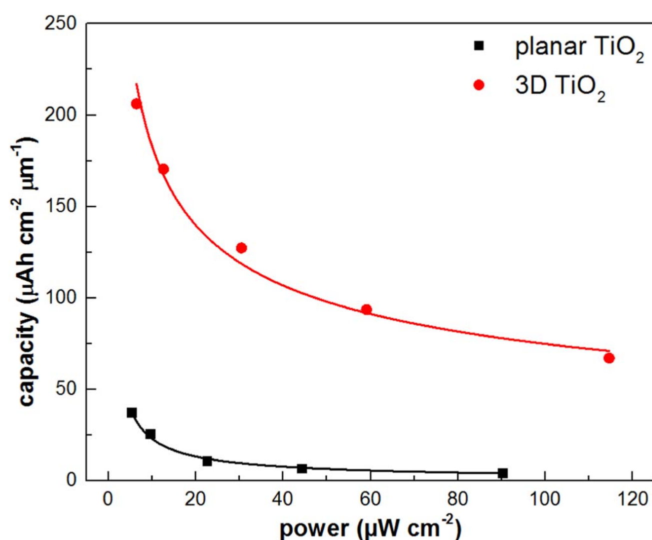

Figure 9. Power and storage capacity comparison of planar and 3D TiO_2 film electrodes.

becomes higher, even exceeding the surface area enlargement. This further manifests the advantage of the 3D electrode geometry in improving the power performance, especially at high (dis)charging current densities.

Fig. 9 shows the energy density as a function of power density for the planar and 3D TiO_2 electrodes. It is clear that at all output powers, the 3D TiO_2 film electrode reveals a higher capacity. Or alternatively, at a given storage capacity, the 3D electrode delivers a much higher power output. Based on the above discussion of electrochemical results, it is clear that by applying the concept of 3D film electrode, the storage capacity and power performance of thin film electrodes can be improved simultaneously.

The cycling performance of 3D and planar TiO_2 film electrodes is shown in Fig. 10. The applied current density per footprint area is 4 $\mu A\ cm^{-2}$. During the entire cycling test, the 3D TiO_2 anode shows much higher storage capacity than the planar electrode. This is mainly attributed to the enlarged surface area, which allows more TiO_2 loaded per footprint area. What's more, up to almost 400 cycles, the 3D electrode doesn't show any significant capacity decay, demonstrating excellent cycle performance.

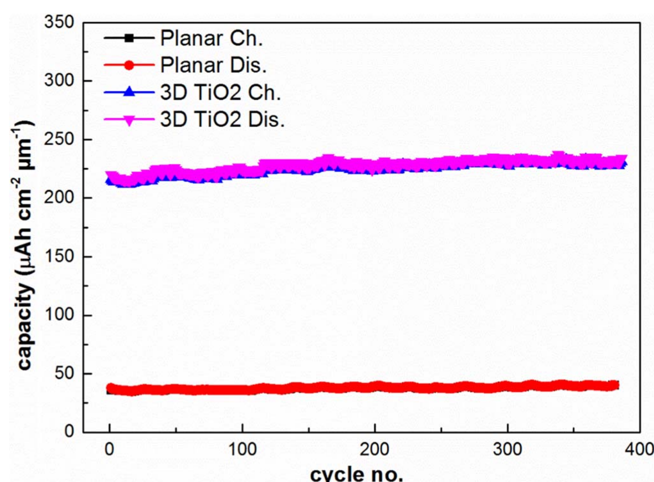

Figure 10. Cycle performances of planar and 3D TiO_2 film electrodes at a current density of 4 $\mu A\ cm^{-2}$.

Conclusions

A flexible and accurate 3D fabrication route to create 3D microbattery electrodes by combining RIE with LPCVD was demonstrated. It has been found that the LPCVD deposition of TiO_2 thin films can be divided into a diffusion-controlled and a kinetically-controlled temperature region. Employing deposition conditions within the kinetically-controlled region, uniform 3D-TiO_2 electrodes have been deposited by LPCVD. Compared with planar TiO_2 electrodes, the storage capacity of 3D-TiO_2 electrodes increased more than 6 times at low current density (4 $\mu A \cdot cm^{-2}$) and even 16 times at high current densities (80 $\mu A \cdot cm^{-2}$). This high storage capacity is maintained even after 450 cycles. Besides the significant improvement of the storage capacity, the power performance is also improved. At all output power densities, the 3D electrodes manifest a higher storage capacity than planar electrodes. The present results open new strategy for depositing electrode materials on complicate 3D-substrates by using LPCVD. It also clearly demonstrates the advantages of 3D electrodes for improving both the storage capacity and power performance of thin film batteries.

Acknowledgments

Imec (Leuven, Belgium) is gratefully acknowledged for providing the 3D pillar substrates for electrochemical test. This work was supported by IWT Flanders (Belgium) under SBO project "SoS-Lion".

References

1. C. Hagleitner, A. Hierlemann, D. Lange, A. Kummer, N. Kerness, O. Brand, and H. Baltes, *Nature*, **414**, 293 (2001).
2. D. C. Bock, A. C. Marschilok, K. J. Takeuchi, and E. S. Takeuchi, *Electrochim. Acta*, **84**, 155 (2012).
3. J. F. M. Oudenhoven, R. J. M. Vullers, and R. Schaijk, *Int. J. Energy Res.*, **36**, 1139 (2012).
4. M. Zougagh and A. Rios, *Analyst*, **134**, 1274 (2009).
5. A. C. Fischer, F. Forsberg, M. Lapisa, S. J. Bleiker, G. Stemme, N. Roxhed, and F. Niklaus, *Microsystems & Nanoengineering*, **1**, 15005 (2015).
6. K. Edström, D. Brandell, T. Gustafsson, and L. Nyholm, *Electrochem. Soc. Interface*, **20**, 41 (2011).
7. P. H. L. Notten, F. Roozeboom, R. A. H. Niessen, and L. Baggetto, *Advanced Materials*, **19** (2007).
8. L. Baggetto, H. C. M. Knoops, R. A. H. Niessen, W. M. M. Kessels, and P. H. L. Notten, *J. Mater. Chem.*, **20**, 3703 (2010).
9. J. W. Long, B. Dunn, D. R. Rolison, and H. S. White, *Chem. Rev.*, **104**, 4463 (2004).
10. J. F. M. Oudenhoven, L. Baggetto, and P. H. L. Notten, *Adv. Energy Mater.*, **1**, 10 (2011).
11. S. Ferrari, M. Loveridge, S. D. Beattie, M. Jahn, R. J. Dashwood, and R. Bhagat, *J. Power Sources*, **286**, 25 (2015).
12. H. L. Ning, J. H. Pikul, R. Y. Zhang, X. J. Li, S. Xu, J. J. Wang, J. A. Rogers, W. P. King, and P. V. Braun, *Proc. Natl. Acad. Sci. U.S.A.*, **112**, 6573 (2015).
13. G. Kim, S. Jeong, J.-H. Shin, J. Cho, and H. Lee, *ACS Nano*, **8**, 1907 (2014).
14. Y. Wang, B. Liu, Q. Li, S. Cartmell, S. Ferrara, Z. D. Deng, and J. Xiao, *J. Power Sources*, **286**, 330 (2015).
15. M. P. Cantao, J. I. Cisneros, and R. M. Torresi, *J. Phys. Chem.*, **98**, 4865 (1994).
16. W. J. Borghols, D. Lutzenkirchen-Hecht, U. Haake, E. R. van Eck, F. M. Mulder, and M. Wagemaker, *PCCP*, **11**, 5742 (2009).
17. W. Wang, M. Tian, A. Abdulagatov, S. M. George, Y.-C. Lee, and R. Yang, *Nano Lett.*, **12**, 655 (2012).
18. S. K. Cheah, E. Perre, M. Rooth, M. Fondell, A. Harsta, L. Nyholm, M. Boman, T. Gustafsson, J. Lu, P. Simon, and K. Edstrom, *Nano Lett.*, **9**, 3230 (2009).
19. B. L. Ellis, P. Knauth, and T. Djenizian, *Adv. Mater.*, **26**, 3368 (2014).
20. S. Moitzheim, C. S. Nimisha, D. Shaoren, J. C. Daire, C. Detavernier, and P. M. Vereecken, *Nanotechnology*, **25**, 504008 (2014).
21. W. Wei, G. Oltean, C.-W. Tai, K. Edstrom, F. Bjorefors, and L. Nyholm, *J. Mater. Chem. A*, **1**, 8160 (2013).
22. D. P. Singh, A. George, R. V. Kumar, J. E. ten Elshof, and M. Wagemaker, *The Journal of Physical Chemistry C*, **117**, 19809 (2013).
23. J. F. M. Oudenhoven, T. v. Dongen, R. A. H. Niessen, M. H. J. M. d. Croon, and P. H. L. Notten, *J. Electrochem. Soc.*, **156**, D169 (2009).
24. J. Xie, J. F. M. Oudenhoven, P. P. R. M. L. Harks, D. J. Li, and P. H. L. Notten, *J. Electrochem. Soc.*, **162**, A249 (2015).
25. J. Xie, P.-P. R. M. L. Harks, D. Li, L. H. J. Raijmakers, and P. H. L. Notten, *Solid State Ionics*, **287**, 83 (2016).
26. F. Laermer and A. Urban, *Microelectron. Eng.*, **67–68**, 349 (2003).
27. T. Ohsaka, F. Izumi, and Y. Fujiki, *Journal of Raman Spectroscopy*, **7**, 321 (1978).
28. A. C. Jones and M. L. Hitchman, *Chemical Vapour Deposition: Precursors, Processes and Applications*, Royal Society of Chemistry (2009).
29. J. L. Cheng, B. Wang, H. L. L. Xin, C. Kim, F. D. Nie, X. D. Li, G. C. Yang, and H. Huang, *J. Mater. Chem. A*, **2**, 2701 (2014).
30. M. Wagemaker, W. J. Borghols, and F. M. Mulder, *J. Am. Chem. Soc.*, **129**, 4323 (2007).